arXiv:1209.5100v1 [cond-mat.str-el] 23 Sep 2012

On the Origin of Zigzag Magnetic Order in Iridium Oxide Na_2IrO_3

Jiří Chaloupka,[1,2] George Jackeli,[1,*] and Giniyat Khaliullin[1]

[1] *Max Planck Institute for Solid State Research, Heisenbergstrasse 1, D-70569 Stuttgart, Germany*
[2] *Central European Institute of Technology, Masaryk University, Kotlářská 2, 61137 Brno, Czech Republic*

(Dated: September 25, 2012)

We explore the phase diagram of spin-orbit Mott insulators on a honeycomb lattice, within the Kitaev-Heisenberg model extended to its full parameter space. Zigzag-type magnetic order is found to occupy a large part of the phase diagram of the model, and its physical origin is explained as due to interorbital $t_{2g} - e_g$ hopping. Magnetic susceptibility and spin wave spectra are calculated and compared to the experimental data, obtaining thereby the spin coupling constants in Na_2IrO_3 and Li_2IrO_3.

PACS numbers: 75.10.Jm, 75.30.Et, 75.25.Dk

In the quest for the materials with novel electronic phases, iridium oxide Na_2IrO_3 came into focus recently [1–7] due to theoretical predictions [8, 9] that this system may host Kitaev model physics and quantum spin Hall effect.

Na_2IrO_3 is an insulator with sizable and temperature independent optical gap $\simeq 0.35$ eV [7], and shows Curie-Weiss type susceptibility [1, 6] with moments corresponding to effective spin one-half of Ir^{4+} ion with t_{2g}^5 configuration [10]. These facts imply that Na_2IrO_3 is a Mott insulator with well localized Ir-moments.

Collective behavior of local moments in Mott insulators is governed by three distinct and often competing forces: (*i*) orbital-lattice (Jahn-Teller) coupling, (*ii*) virtual hopping of electrons across the Mott gap resulting in exchange interactions, and (*iii*) relativistic spin-orbit coupling (see Ref. [11] for extensive discussions). The corresponding energy scales E_{JT}, J, and λ vary broadly depending on the type of magnetic ions and chemical bonding [12]. When $\lambda > (E_{JT}, J)$, as often realized for Co, Rh, Ir ions in octahedral environment, local moments acquire a large orbital component which may result in a strong departure from spin-only Heisenberg models [8, 11]. The direct observation of large spin-orbit splitting $3\lambda/2 \sim 0.6 - 0.7$ eV in insulating iridates Sr_2IrO_4 [13], $Sr_3Ir_2O_7$ [14], and Na_2IrO_3 [15] made it certain that $\lambda > (E_{JT}, J)$. Thus, low-energy physics of Na_2IrO_3 is governed by interactions among the spin-orbit entangled Kramers doublets of Ir-ions.

It is also established now [3–5] that Ir-moments in Na_2IrO_3 undergo antiferromagnetic (AF) order at $T_N \simeq 15$ K. The fact that T_N is much smaller than paramagnetic Curie temperature (-125 K) [6] and spin-wave energies [4] implies that the underlying interactions are strongly frustrated. This is natural in so-called Kitaev-Heisenberg (KH) model [16] where long range order is suppressed by the proximity to the Kitaev spin-liquid (SL) state. However, the observed "zigzag" magnetic pattern [ferromagnetic (FM) zigzag chains, AF-coupled to each other] came as a surprising challenge to this simple and attractive model. To resolve the "zigzag puzzle", various proposals, ranging from routine extensions of the KH model [6, 17, 18] to a complete denial [19] of the presence of local Ir-moments, have been put forward.

In this Letter, we show that the zigzag order is in fact a natural ground state (GS) of the KH model, in a previously overlooked parameter range. Next, we identify the exchange process that supports a zigzag-phase regime. Further, we calculate spin-wave spectra and magnetic susceptibility of the model in zigzag phase, and find a nice agreement with experiments [1, 4, 6]. This lends strong support to the KH model as a dominant interaction in Na_2IrO_3 and related oxides.

The model.– Nearest-neighbor (NN) interaction between isospin one-half Kramers doublets of Ir^{4+} ions, coupled via 90°-exchange bonds, reads as follows (the exchange processes are described later):

$$\mathcal{H}_{ij}^{(\gamma)} = 2K\ S_i^\gamma S_j^\gamma + J\ \boldsymbol{S}_i \cdot \boldsymbol{S}_j\ . \qquad (1)$$

Here, $\gamma (= x, y, z)$ labels 3 distinct types of NN bonds of a honeycomb lattice [16] of Ir ions in Na_2IrO_3, and spin axes are oriented along the Ir-O bonds of IrO_6 octahedron. The bond-dependent Ising coupling between the γ components of spins is nothing but Kitaev model [20], and the second term stands for the Heisenberg exchange.

Let us introduce the energy scale $A = \sqrt{K^2 + J^2}$ and the angle φ via $K = A \sin\varphi$ and $J = A\cos\varphi$; the model (1) takes then the following form:

$$\mathcal{H}_{ij}^{(\gamma)} = A\ (2\sin\varphi\ S_i^\gamma S_j^\gamma + \cos\varphi\ \boldsymbol{S}_i \cdot \boldsymbol{S}_j). \qquad (2)$$

We let the "phase" angle φ to vary from 0 to 2π, uncovering thereby additional phases of the model that escaped attention previously [16], including its zigzag ordered state which is of a particular interest here.

It is highly instructive to introduce, following Refs. [11, 16], 4 sublattices with the fictitious spins $\tilde{\boldsymbol{S}}$, which are obtained from $\boldsymbol{S}$ by changing the sign of its two appropriate components depending on the sublattice index. This transformation (generic for triangular, honeycomb, kagome lattices) results in the $\tilde{\boldsymbol{S}}$-Hamiltonian of the same form as (1), but with effective couplings $\tilde{K} = K + J$

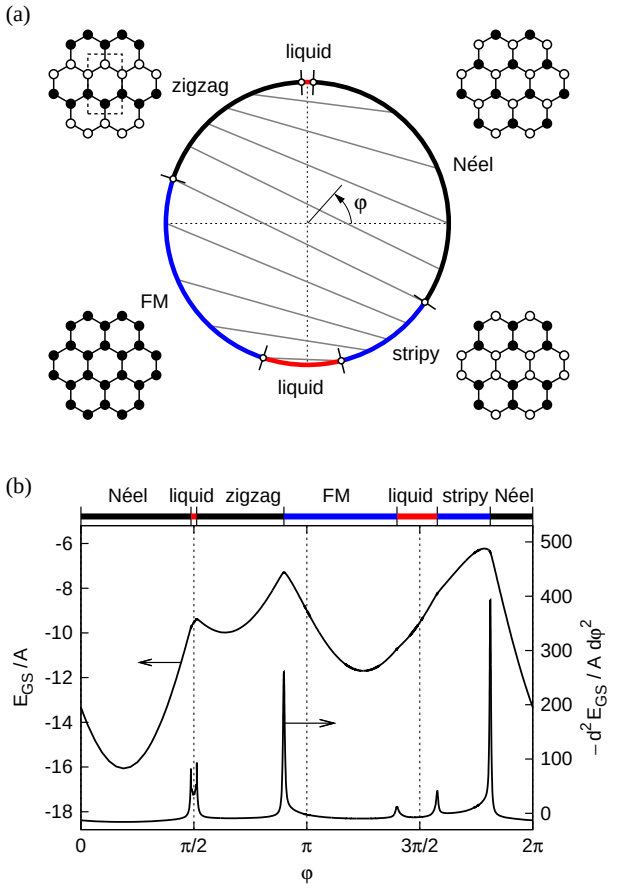

FIG. 1: (color online). (a) Phase diagram of the Kitaev-Heisenberg model containing 2 spin-liquid and 4 spin-ordered phases. The transition points (open dots on φ-circle) are obtained by an exact diagonalization. The gray lines inside the circle connect the points related by the exact mapping (see text). Open/solid circles in the insets indicate up/down spins. The rectangular box in zigzag pattern (top-left) shows the magnetic unit cell. (b) Groundstate energy $E_{\rm GS}$ of 24-site cluster and its second derivative $-{\rm d}^2E_{\rm GS}/{\rm d}\varphi^2$ revealing the phase transitions.

and $\tilde{J}=-J$, revealing a hidden $SU(2)$ symmetry of the model at $K=-J$ (where the Kitaev term $\tilde{K}$ vanishes). For the angles, the mapping reads as $\tan\tilde{\varphi}=-\tan\varphi-1$.

Phase diagram.– In its full parameter space, the KH model accommodates 6 different phases, best visualized using the phase-angle φ as in Fig. 1(a). In addition to the previously discussed [16, 21, 22] Néel-AF, stripy-AF, and SL states near $\varphi=0$, $-\frac{\pi}{4}$, and $-\frac{\pi}{2}$, respectively, we observe 3 more states. First one is "AF" ($K>0$) Kitaev spin-liquid near $\varphi=\frac{\pi}{2}$. Second, FM phase broadly extending over the third quadrant of the φ-circle. The FM and stripy-AF states are connected [see Fig. 1(a)] by the 4-sublattice transformation, which implies their identical dynamics. Finally, near $\varphi=\frac{3}{4}\pi$, the most wanted phase, zigzag-AF, appears occupying almost a quarter of the phase space. Thanks to the above mapping, it is understood that the zigzag and Néel states are isomorphic, too. In particular, the $\varphi=\frac{3}{4}\pi$ zigzag is identical to Heisenberg-AF of the fictitious spins.

To obtain the phase boundaries, we have diagonalized the model numerically, using a hexagonal 24-site cluster with periodic boundary conditions. The cluster is compatible with the above 4-sublattice transformation and $\varphi\leftrightarrow\tilde{\varphi}$ mapping. As seen in Fig. 1(b), the second derivative of the GS energy $E_{\rm GS}$ with respect to φ well detects the phase transitions. Three pairs of linked transition points are found: $(87.7°, 92.2°)$ and $(-76.1°, -108.2°)$ for the spin liquid/order transitions around $\pm\frac{\pi}{2}$, and $(161.7°, -33.8°)$ for the transitions between ordered phases.

The transitions from zigzag-AF to FM, and from stripy-AF to Néel-AF are of first order by symmetry; see very sharp peaks in Fig. 1(b). The spin liquid/order transitions near $\varphi=-\frac{\pi}{2}$ lead to wider and much less pronounced peaks, suggesting a second (or weakly first) order transition [16]. On the contrary, liquid/order transitions around $\varphi=\frac{\pi}{2}$ show up as very narrow peaks; on the finite cluster studied, they correspond to real level crossings. Nature of these quantum phase transitions remains to be clarified.

While at $J=0$ (i.e. $\varphi=\pm\frac{\pi}{2}$) the sign of K is irrelevant [20], the stability of the AF- and FM-type Kitaev spin-liquids against J-perturbation is very different: the SL phase near $\frac{\pi}{2}$ ($-\frac{\pi}{2}$) is less (more) robust. This phase behavior is related to a different nature of the competing ordered phases: for the $\frac{\pi}{2}$ SL, these are highly quantum zigzag and Néel states, while the SL near $-\frac{\pi}{2}$ is sandwiched by more classical (FM and "fluctuation free" stripy [16]) states which are energetically less favorable than quantum SL state.

Exchange interactions in Na_2IrO_3.– Having fixed the parameter space ($K>0, J<0$) for zigzag phase, we turn now to the physical processes behind the model (1). Interactions between local moments in Mott insulators arise due to virtual hoppings of electrons. This may happen in many different ways, depending sensitively on chemical bonding, intra-ionic electron structure, etc. The case of present interest (i.e., strong spin-orbit coupling, t_{2g}^5 configuration, and 90°-bonding geometry) has been addressed in several papers [8, 11, 16, 23]. There are following four physical processes that contribute to K and J couplings.

Process 1: Direct hopping t' between NN t_{2g} orbitals. Since no oxygen orbital is involved, 90°-bonding is irrelevant; the resulting Hamiltonian is $H_1=I_1\,\boldsymbol{S}_i\cdot\boldsymbol{S}_j$ with $I_1\simeq(\frac{2}{3}t')^2/U$ [16]. Here, U is Coulomb repulsion between t_{2g} electrons. Typically, one has $t'/t<1$, when compared to the indirect hopping t of t_{2g} orbitals via oxygen ions.

Process 2: Interorbital NN $t_{2g}-e_g$ hopping $\tilde{t}$. This is the dominant pathway in 90°-bonding geometry since it involves strong $t_{pd\sigma}$ overlap between oxygen-$2p$ and e_g or-

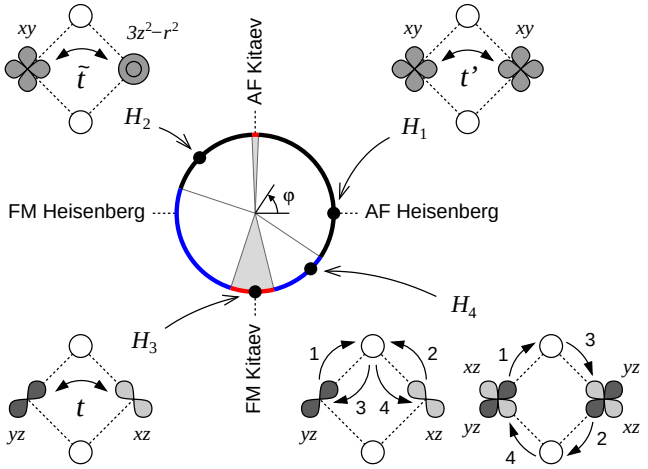

FIG. 2: (color online). Schematics of 4 different exchange processes (see text for details), arranged around the φ-phase diagram of Fig. 1(a). Taken separately, the Hamiltonians H_1, H_2, H_3, and H_4 would favor "pure" Néel-AF, zigzag-AF, Kitaev-SL, and stripy-AF states, respectively, as indicated by arrows connecting H_i with the dots on φ-circle. The circle is divided into the phase-sectors by gray lines; SL phases are shaded.

bital; typically, $\tilde{t}/t \sim 2$. The corresponding Hamiltonian is [11]:

$$H_2^{(\gamma)} = I_2\ (2S_i^\gamma S_j^\gamma - \boldsymbol{S}_i \cdot \boldsymbol{S}_j). \qquad (3)$$

This is nothing but the model (1) with $K = -J = I_2 > 0$, i.e., at its SU(2) symmetric point $\varphi = \frac{3}{4}\pi$ inside the zigzag phase, see Fig. 2. For the Mott-insulating iridates (as opposed to charge-transfer cobaltates [11]), we estimate $I_2 \simeq \frac{4}{9}(\tilde{t}/\tilde{U})^2 \tilde{J}_H$, where $\tilde{U}$ is (optically active) excitation energy associated with $t_{2g} - e_g$ hopping, and $\tilde{J}_H$ is Hund's interaction between t_{2g} and e_g orbitals. The physics behind this expression is clear: $(\tilde{t}/\tilde{U})^2$ measures the amount of t_{2g} spin which is transferred to NN e_g orbital; once arrived, it encounters the "host" t_{2g} spin and has to obey the Hund's rule.

For its remarkable properties, the Hamiltonian H_2 (3) deserves a few more words. On a triangular lattice, it shows a nontrivial spin vortex ground state (see Fig. 5 of Ref. [11]); however, the elementary excitations are simple $SU(2)$ magnons of a conventional Heisenberg-AF. When regarded as "J"-part of a doped $t-J$ model, it leads to an exotic pairing [11, 24].

Process 3: Indirect hopping t between NN t_{2g} orbitals via two intermediate oxygen ions. This gives rise to the Kitaev model $H_3^{(\gamma)} = -I_3 S_i^\gamma S_j^\gamma$, with $I_3 \simeq \frac{8}{3}(t^2/U)(J_H/U)$ [8] where J_H is Hund's coupling between t_{2g} electrons. This process supports $\varphi = -\frac{\pi}{2}$ SL state, see Fig. 2.

Process 4: Mechanisms involving pd charge-transfer excitations (energy Δ_{pd}). Two holes may meet at an oxygen (and experience U_p repulsion), or cycle around a Ir_2O_2 plaquette (Fig. 2). The corresponding Hamiltonian H_4 [8, 11, 23] has the form as of H_2 (3). The coupling constant $I_4 \simeq \frac{8}{9}(\frac{1}{\Delta_{pd}+U_p/2} - \frac{1}{\Delta_{pd}})$ turns out to be negative because of the near cancellation of the two terms [8, 25]. It thus supports stripy-AF not observed in Na_2IrO_3.

Putting things together, we observe that it is the interorbital $t_{2g} - e_g$ hopping H_2 process that uniquely supports zigzag order. This implies also that multiorbital Hubbard-type models, when applied to iridates with 90°-bonding geometry, must include e_g states as well, even though the moments reside predominantly in the t_{2g} shell.

Up to this point, we neglected trigonal field splitting Δ of the t_{2g} level due to the c-axis compression present in Na_2IrO_3. This approximation is valid as long as Δ is much smaller than spin-orbit coupling $\lambda \simeq 0.4$ eV [13, 26] and seems to be justified, since the recent *ab-initio* calculations [19] suggest that $\Delta \simeq 75$ meV only [27].

We have also examined the longer-range couplings, using the hopping matrix of Ref. [19], and found that second-NN interaction has the form of (3) (as noticed previously [28]), while third-NN interaction is of AF-Heisenberg type. The second (third)-NN interaction would oppose (support) zigzag order; however, we believe that these couplings are not significant in Na_2IrO_3 because the corresponding long-range hoppings are found to be small [19, 29].

We do not attempt here to evaluate the parameters involved in H_1–H_4; *ab-initio* calculations as in Ref. [30] might be more useful in this regard. Instead, having obtained a zigzag order in our model (1) and identified the physical process driving this order, we turn now to the experimental data. The J and K values in Na_2IrO_3 and Li_2IrO_3 will be extracted below from analysis of the neutron scattering and magnetic susceptibility data.

Spin-waves in the zigzag phase.– Consider a single domain zigzag state, e.g., with FM chains running perpendicular to z-type bonds. Following Ref. [4], we introduce a rectangular $a \times b$ magnetic unit cell [$\sqrt{3}a_0 \times 3a_0$ in terms of hexagon-edge a_0, see Fig. 1(a)], and define the ab-plane wave vector $\mathbf{q}$ in units of (h,k) as $\mathbf{q} = (\frac{2\pi}{a}h, \frac{2\pi}{b}k)$. Standard spin-wave theory gives four dispersive branches:

$$\omega_{1,2}^2(h,k) = \left[K^2 + (K+J)^2\right] c_h^2 - KJ(1 - s_h s_k) \\ \pm |(K+J)c_h| \sqrt{(2K-J)^2 - (2Ks_h - Js_k)^2}\ , \qquad (4)$$

and $\omega_{3,4}(h,k) = \omega_{1,2}(-h,k)$, with $c_h = \cos\pi h$, $s_h = \sin\pi h$, and $s_k = \sin\pi k$. If $K = -J$, i.e. at $\varphi = \frac{3}{4}\pi$ point of hidden $SU(2)$ symmetry, two branches are degenerate ($\omega_1 = \omega_2$) and become true Goldstone modes. Away from this special point, small magnon gap is expected to open by quantum effects not considered here. For $\mathbf{q}$ with $h = k$, the spin-wave dispersions (4) simplify to $\omega_1(h,h) = \sqrt{2K(2K+J)}\ |c_h|$ and $\omega_2(h,h) = \sqrt{2}|Jc_h|$, revealing two different energy scales in magnon spectra

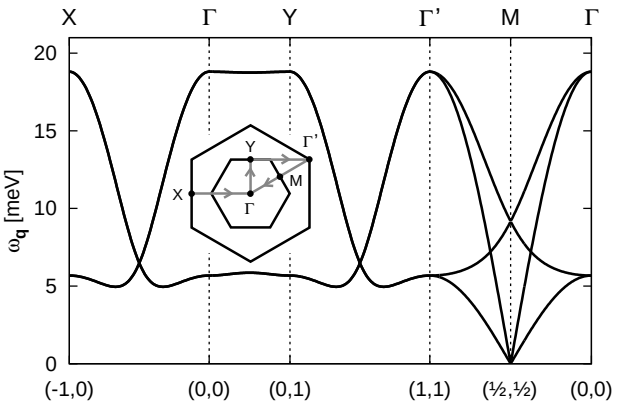

FIG. 3: Magnon spectra in the zigzag phase calculated using Eq. (4) with $(J, K) = (-4.01, 10.45)$ meV. The inset shows the path along the symmetry directions in the reciprocal space; notations of Ref. [4] are used.

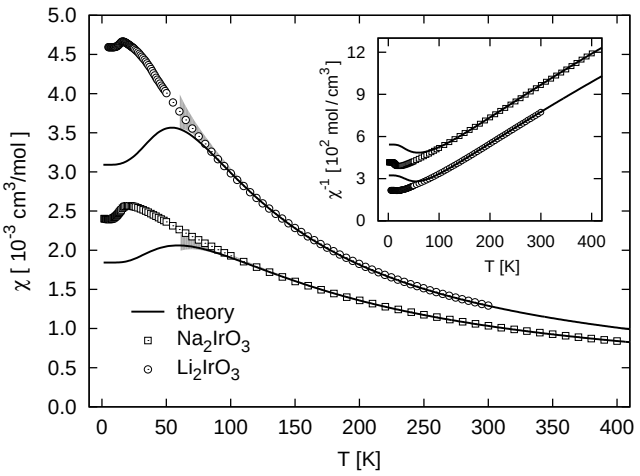

FIG. 4: Experimental magnetic susceptibilities for Na_2IrO_3 [1, 6] (squares) and Li_2IrO_3 [6] (circles) fitted by theoretical results calculated with $(J, K) = (-4.01, 10.45)$ meV and $(-5.30, 7.85)$ meV, respectively. Exact χ of the 8-site cluster is shown as solid lines. Lanczos results for the 24-site cluster are indicated by shading [32]. Their comparison suggests that the calculated χ gives the thermodynamic limit down to $T \approx 100$ K where the finite-size effects become significant.

set by K and J couplings.

While the bandwidth of the lowest dispersive mode (set by J) is already known to be about 5-6 meV [4], we are not aware of the high energy magnon data to estimate K in Na_2IrO_3. We have therefore examined (see below) the magnetic susceptibility data [1, 6], and obtained $(J, K) = (-4.01, 10.45)$ meV that well fit the susceptibility as well as neutron scattering data [4]. With this, we predict magnon spectra for Na_2IrO_3 shown in Fig. 3. The lowest dispersive (J) mode is as observed [4], indeed. However, mapping out entire magnon spectra is highly desirable to quantify the Kitaev term K directly.

Magnetic susceptibility .– We have calculated the uniform magnetic susceptibility $\chi(T)$ of the model (1) on 8-site cluster (using full exact diagonalization) and 24-site cluster (using finite-temperature Lanczos method [31, 32]). Both clusters are compatible with the zigzag order when periodic boundary conditions are applied. The parameters are varied such that $J = A\cos\varphi$ is consistent with the neutron data [4] while φ stays within the zigzag sector of Fig. 1(a); this strongly narrows the possible K-window. For the data fits, we let g-factor of Ir^{4+} ion to deviate from 2 (due to the covalency effects [10]), and include T-independent Van Vleck term χ_0. The result for $J = -4.01$ meV, $K = 10.45$ meV, $g = 1.78$, $\chi_0 = 0.16 \times 10^{-3}$cm^3/mol fits the Na_2IrO_3 data nicely (Fig. 4); deviations occur at low temperatures only, when correlation length exceeds the size of the cluster used. The fit is quite robust: similar results can be found for small only variations, locating Na_2IrO_3 near $\varphi = 111 \pm 2°$ of the model phase diagram Fig.1(a). The spin couplings obtained are reasonable for the 90°-exchange bonds (as expected [8, 11], they are much smaller than in 180°-bond perovskites [13, 14]). The magnitude of Van Vleck term also agrees with our estimate $\chi_0 \simeq \frac{8}{3\lambda}\mu_B^2 N_A \simeq 0.2 \times 10^{-3}$ cm^3/mol for Ir^{4+} ion, considering spin-orbit coupling $\lambda \simeq 0.4$ eV [13, 26].

For the sake of curiosity, we have also fitted $\chi(T)$ data of Li_2IrO_3 [6], a sister compound of Na_2IrO_3. Acceptable results have been found for the angle window $\varphi = 124 \pm 6°$; a representative plot for $J = -5.30$ meV, $K = 7.85$ meV, $g = 1.94$, $\chi_0 = 0.14 \times 10^{-3}$ cm^3/mol is shown in Fig. 4. It is worth noticing that the value of J, which controls the bandwidth of the softest spin-wave mode (see Fig. 3), appears to be similar in both compounds. This may explain why they undergo magnetic transition at similar $T_N \simeq 15$ K, despite very different high temperature susceptibilities.

To conclude, we have clarified the origin of zigzag magnetic order in Na_2IrO_3 in terms of nearest-neighbor Kitaev-Heisenberg model for localized Ir-moments. The model well agrees with the low-energy magnon and high temperature magnetic susceptibility data. A general implication of this work is that the interactions considered here should hold a key for understanding the magnetism of a broad class of spin-orbit Mott insulators with 90°-exchange bonding geometry, including triangular, honeycomb, hyperkagome lattice iridates.

We thank R. Coldea, Y. Singh, and H. Takagi for discussions. JC acknowledges support by the Alexander von Humbolt Foundation, ERDF under project CEITEC (CZ.1.05/1.1.00/02.0068), and EC 7th Framework Programme (286154/SYLICA). GJ is supported by GNSF/ST09-447 and in part by the NSF under Grant No. NSF PHY11-25915.

* Also at Andronikashvili Institute of Physics, 0177 Tbilisi, Georgia

[1] Y. Singh and P. Gegenwart, Phys. Rev. B **82**, 064412 (2010).

[2] H. Takagi (unpublished).

[3] X. Liu, T. Berlijn, W.-G. Yin, W. Ku, A. Tsvelik, Y.-J. Kim, H. Gretarsson, Y. Singh, P. Gegenwart, and J.P. Hill, Phys. Rev. B **83**, 220403 (2011).

[4] S.K. Choi, R. Coldea, A.N. Kolmogorov, T. Lancaster, I.I. Mazin, S.J. Blundell, P.G. Radaelli, Y. Singh, P. Gegenwart, K.R. Choi, S.-W. Cheong, P.J. Baker, C. Stock, and J. Taylor, Phys. Rev. Lett. **108**, 127204 (2012).

[5] F. Ye, S. Chi, H. Cao, B.C. Chakoumakos, J.A. Fernandez-Baca, R. Custelcean, T.F. Qi, O.B. Korneta, and G. Cao, Phys. Rev. B **85**, 180403 (2012).

[6] Y. Singh, S. Manni, J. Reuther, T. Berlijn, R. Thomale, W. Ku, S. Trebst, and P. Gegenwart, Phys. Rev. Lett. **108**, 127203 (2012).

[7] R. Comin, G. Levy, B. Ludbrook, Z.-H. Zhu, C.N. Veenstra, J.A. Rosen, Y. Singh, P. Gegenwart, D. Stricker, J.N. Hancock, D. van der Marel, I.S. Elfimov, and A. Damascelli, arXiv:1204.4471.

[8] G. Jackeli and G. Khaliullin, Phys. Rev. Lett. **102**, 017205 (2009).

[9] A. Shitade, H. Katsura, J. Kuneš, X.-L. Qi, S.-C. Zhang, and N. Nagaosa, Phys. Rev. Lett. **102**, 256403 (2009).

[10] A. Abragam and B. Bleaney, *Electron Paramagnetic Resonance of Transition Ions* (Clarendon Press, Oxford, 1970).

[11] G. Khaliullin, Prog. Theor. Phys. Suppl. **160**, 155 (2005).

[12] J.B. Goodenough, *Magnetism and the Chemical Bond* (Interscience, New York, 1963).

[13] J. Kim, D. Casa, M.H. Upton, T. Gog, Y.-J. Kim, J.F. Mitchell, M. van Veenendaal, M. Daghofer, J. van den Brink, G. Khaliullin, and B.J. Kim, Phys. Rev. Lett. **108**, 177003 (2012).

[14] J. Kim, A.H. Said, D. Casa, M.H. Upton, T. Gog, M. Daghofer, G. Jackeli, J. van den Brink, G. Khaliullin, B.J. Kim, Phys. Rev. Lett. (in press); arXiv:1205.5337.

[15] Y.-J. Kim *et al.*, (unpublished).

[16] J. Chaloupka, G. Jackeli, and G. Khaliullin, Phys. Rev. Lett. **105**, 027204 (2010).

[17] I. Kimchi and Y.-Z. You, Phys. Rev. B **84**, 180407 (2011).

[18] S. Bhattacharjee, S.-S. Lee, and Y.B. Kim, New J. Phys., **14**, 073015 (2012).

[19] I.I. Mazin, H.O. Jeschke, K. Foyevtsova, R. Valenti, and D.I. Khomskii, arXiv:1205.0434.

[20] A. Kitaev, Ann. Phys. (N.Y.) **321**, 2 (2006).

[21] H.-C. Jiang, Z.-C. Gu, X.-L. Qi, and S. Trebst, Phys. Rev. B **83**, 245104 (2011).

[22] J. Reuther, R. Thomale, and S. Trebst, Phys. Rev. B **84**, 100406 (2011).

[23] G. Chen and L. Balents, Phys. Rev. B **78**, 094403 (2008).

[24] G. Khaliullin, W. Koshibae, and S. Maekawa, Phys. Rev. Lett. **93**, 176401 (2004).

[25] The results for I_4 of Refs. [11, 23] were incomplete.

[26] O.F. Schirmer, A. Forster, H. Hesse, M. Wohlecke, and S. Kapphan, J. Phys. C **17**, 1321 (1984).

[27] Typically, "noncubic" corrections to the interactions between Kramers doublets scale as $(\frac{3\cos 2\theta-1}{2})^2$ [24] which is about 0.01 if $\Delta = 75$ meV. [θ is given by $\tan 2\theta = 2\sqrt{2}\lambda/(\lambda+2\Delta)$]. The case of $\Delta > \lambda$ can be excluded also on the grounds that, in this limit, the interactions become *bond-independent* and support either Ising-FM or xy-AF states [11].

[28] J. Reuther, R. Thomale, and S. Rachel, arXiv:1206.3103.

[29] E.g., the second-NN hopping ~ 75 meV is about 4 times less than NN hopping t via oxygen [19]; note that hopping matrix elements enter in spin couplings quadratically.

[30] V.M. Katukuri, H. Stoll, J. van den Brink, and L. Hozoi, Phys. Rev. B **85**, 220402(R) (2012).

[31] J. Jaklič and P. Prelovšek, Adv. Phys. **49**, 1 (2000).

[32] The finite-temperature Lanczos method was performed using $M = 100$ Lanczos steps and $N_{\rm st} = 1024$ random sampling vectors. The values of χ and their statistical error are presented in Fig. 4 in the form of 3σ-intervals estimated by taking many different sets of the sampling vectors.